Journal of Nuclear Materials 400 (2010) 213–217

Contents lists available at ScienceDirect

Journal of Nuclear Materials

journal homepage: www.elsevier.com/locate/jnucmat

Thermal diffusivity of homogeneous SBR MOX fuel with a burn-up of 35 MWd/kgHM

C. Cozzo [a], D. Staicu [a,*], G. Pagliosa [a], D. Papaioannou [a], V.V. Rondinella [a], R.J.M. Konings [a], C.T. Walker [a], M.A. Barker [b], P. Hervé [c]

[a] European Commission, Joint Research Centre, Institute for Transuranium Element, P.O. Box 2340, D-76125 Karlsruhe, Germany
[b] The UK's National Nuclear Laboratory Ltd., Central Laboratory, Sellafield, Seascale, Cumbria CA20 1PG, UK
[c] LEEE, University Paris X, 1 Chemin Desvalliere, 92410 Ville d'Avray, France

ARTICLE INFO

Article history:
Received 1 February 2010
Accepted 10 March 2010

ABSTRACT

The effect of burn-up on the thermal conductivity of homogeneous SBR MOX fuel is investigated and compared with standard UO_2 LWR fuel. New thermal diffusivity results obtained on SBR MOX fuel with a pellet burn-up of 35 MWd/kgHM are reported. The thermal diffusivity measurements were carried out at three radial positions using a shielded "laser-flash" device and show that the thermal diffusivity increases from the pellet periphery to the centre. The fuel thermal conductivity was found to be in the same range as for UO_2 of similar burn-up. The annealing behaviour was characterized in order to identify the degradation due to the out-of-pile auto-irradiation.

1. Introduction

Uranium–plutonium mixed oxide fuel (MOX) represents about 30% of the nuclear fuel used in commercial light water reactors (LWR). The plutonium is recovered during the reprocessing of spent LWR uranium oxide fuel. The production of MOX fuel, obtained by mixing a few percent of plutonium oxide with UO_2, contributes to the closure of the nuclear fuel cycle by re-using fissile plutonium instead of disposing of it as waste. It also helps reduce the stockpiles of plutonium. Various industrial processes are used for its production, leading to different microstructures mainly characterised by the degree of homogeneity of the plutonium distribution. The introduction of plutonium in UO_2 and the impact of the different microstructures need to be investigated from the point of view of in-pile fuel performance. Systematic studies of the thermal properties of the un-irradiated fuel [1,2] have shown that the thermal conductivity is considerably lower than that of UO_2 and that the effect of the Pu concentration is insignificant in the range 3–15 wt.%. This degradation is therefore difficult to attribute to the effect of the Pu only and it has been proposed that the deviation from stoichiometry is the main cause [3]. The effects of burn-up on the fuel operating temperature and thermal conductivity also need to be established. At present, empirical estimations [4] are used, based on a conservative approach that assumes that the conductivity ratio between UO_2 and MOX is constant with burn-up and equal to the ratio of the fresh fuels. Direct in-pile central temperature measurements have been published by Fujii et al. [5] and analysed on the assumption that the burn-up degradation in MOX is slightly lower than that in UO_2; however, the authors indicate that further investigations are necessary. Direct thermal diffusivity measurements on irradiated MOX fuel and a comparison with UO_2 fuel of equivalent burn-up are presented in the current paper in order to clarify this matter. In the following sections, the samples, the experimental procedure and the results for the thermal diffusivity and thermal conductivity of SBR MOX fuel are described. These results are then compared with the literature data for UO_2 and other heterogeneous MOX fuel variants.

2. Samples

The results reported were obtained in the frame of the first commercial irradiation of short binderless route (SBR) homogeneous MOX fuel which was manufactured at Sellafield, UK. The irradiation took place over the period 1994–1997 in assembly M501 in the Beznau-1 PWR, Switzerland. MOX fuel rods with burn-ups in the range 31–36 MWd/kgHM were sent for post-irradiation examination at the Institute for Transuranium Elements (ITU). In previous publications the microstructure and fission gas release results were described [6,7]. The fuel on which the thermal diffusivity measurements were made had a pellet burn-up of 35 MWd/kgHM. The plutonium content of the fresh fuel was 3.7 wt.% and the volume fraction of the Pu-rich areas (Pu concentration above 20 wt.%) was less than 2%, confirming the high homogeneity of the plutonium distribution in the fresh fuel. The radial burn-up distribution was measured by EPMA and was found to be almost flat. The radial temperature distribution during the

* Corresponding author.
E-mail address: dragos.staicu@ec.europa.eu (D. Staicu).

0022-3115/$ - see front matter © 2010 Elsevier B.V. All rights reserved.
doi:10.1016/j.jnucmat.2010.03.006

last irradiation cycle, required for the interpretation of the thermal diffusivity data, was calculated using the ENIGMA code [8].

3. Experimental procedure

The thermal diffusivity measurements were carried out using a shielded laser flash device, designed and constructed at ITU for highly γ-active materials [9]. The sample is heated at the measurement temperature in a high frequency furnace under nitrogen atmosphere of 10^{-2} mbar, in the temperature range from 520 to 1460 K. Preliminary tests consisting in samples oxygen potential measurements before and after the measurements have shown that under these conditions the oxygen content of fresh and irradiated MOX fuel was not modified. The samples were fragments of a disc, with a thickness of about 1 mm, and with lateral dimensions between 3 and 5 mm. These discs were cut from fuel segments, using a double blade device to ensure parallel faces. Optical pictures of the two faces of the disc were made in order to obtain information about the distribution of the cracks. The fuel was slowly pushed out of the cladding, and fragments were obtained after this operation. The position and orientation of the fragments used for the measurement were accurately determined. The faces were checked to ensure that they were plane and parallel, without cracks. The local thermal diffusivity was measured at different radial positions by moving the pyrometer field-stop aperture (500 μm radius) by step motors across the optical image of the specimen surface produced by a macro-objective. The thermogram for each measurement was carefully inspected to ensure that heat transfer conditions were standard. The presence of perturbations due to internal defects, such as voids and cracks, could be unambiguously detected. The precision of the individual thermal diffusivity measurements is always better than 2%, and the accuracy is of 5%, due to sample thickness variations.

4. Results

4.1. Thermal diffusivity

Starting at about 520 K, seven thermal diffusivity measurement cycles were completed, with increasing maximum temperatures: 630, 750, 830, 930, 1080, 1260 and 1460 K. The experimental thermal history includes the furnace temperature stabilisation time, ranging from about 90 min at 520 K to 20 min at 1460 K, and a measurement time of about 10 min at each temperature (three laser shots). The sample was particularly resistant to fracture and annealing could be performed at temperatures much higher than the local in-pile irradiation temperature during the final cycle without failure. At each investigated temperature, the dependence of the thermal diffusivity on radial position was quantified by making measurements at: $r/r_0 = 0.8$, 0.6 and 0.4. The local irradiation temperatures during the last irradiation cycle were about 880, 1000 and 1080 K and the local burn-ups were 34.9, 32.2 and 30.4 MWd/kgHM, respectively. The measurement results are shown in Figs. 1–3. An increase, that is a recovery, in the thermal

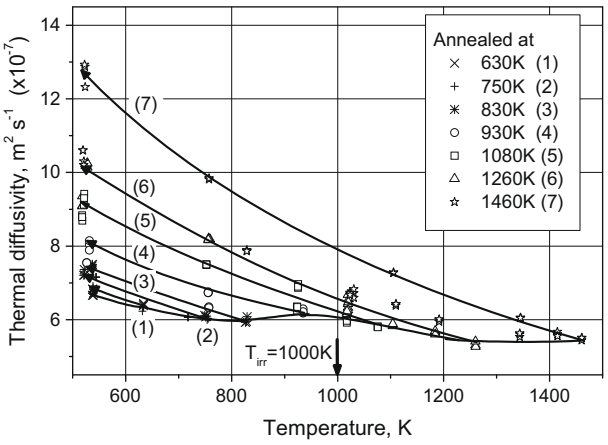

Fig. 2. Thermal diffusivity measurements at relative radius $r/r_0 = 0.6$.

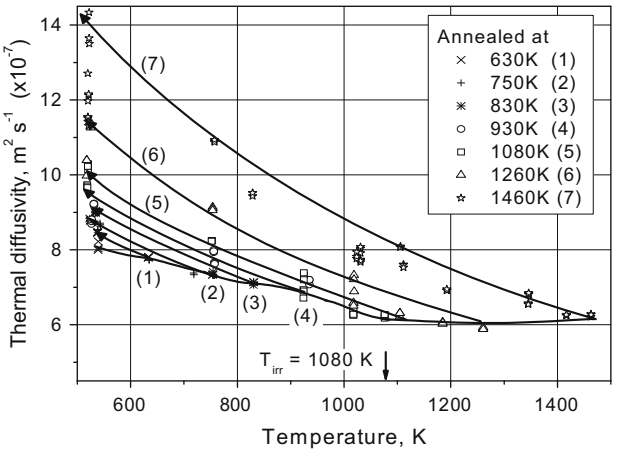

Fig. 3. Thermal diffusivity measurements at relative radius $r/r_0 = 0.4$.

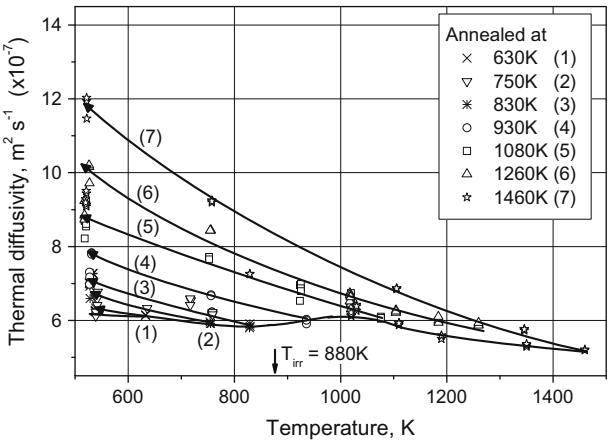

Fig. 1. Thermal diffusivity measurements at relative radius $r/r_0 = 0.8$.

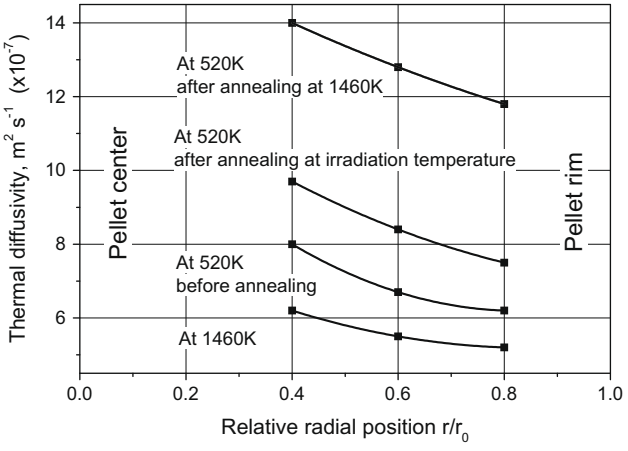

Fig. 4. Thermal diffusivity measurements as a function of the radial position.

Table 1
Coefficients obtained by fitting the measured thermal diffusivity to the expression $1/(A + BT)$.

Temperature range (K)	Position r/r_0	A ($s \times m^{-2}$)	B ($s \times m^{-2} \times K^{-1}$)	A ($s \times m^{-2}$)	B ($s \times m^{-2} \times K^{-1}$)
		Ascending temperature		Descending temperature	
520–630 (run 1)	0.8	1.4038×10^6	3.5446×10^2	1.4213×10^6	3.2672×10^2
	0.6	1.0185×10^6	8.5296×10^2	1.1039×10^6	7.1822×10^2
	0.4	9.8305×10^5	4.7163×10^2	6.1532×10^5	1.0524×10^3
520–750 (run 2)	0.8	8.9702×10^5	9.0370×10^2	9.9705×10^5	7.6255×10^2
	0.6	9.8050×10^5	9.2294×10^2	7.1510×10^5	1.2539×10^3
	0.4	6.9621×10^5	9.1230×10^2	5.9897×10^5	1.0206×10^3
500–830 (run 3)	0.8	9.5428×10^5	9.3675×10^2	7.7035×10^5	1.1337×10^3
	0.6	8.6077×10^5	1.0025×10^2	7.1953×10^5	1.1489×10^3
	0.4	6.6407×10^5	9.0432×10^2	5.7441×10^5	1.0018×10^3
520–930 (run 4)	0.8	1.0542×10^6	6.8330×10^2	7.6390×10^5	9.7002×10^2
	0.6	9.8112×10^5	7.0567×10^2	7.7946×10^5	8.9810×10^2
	0.4	8.1667×10^5	6.2983×10^2	6.7310×10^5	7.7358×10^2
520–1080 (run 5)	0.8	7.6379×10^5	7.8130×10^2	6.4796×10^5	9.0011×10^2
	0.6	5.9355×10^5	1.0613×10^3	4.5931×10^5	1.1564×10^3
	0.4	4.7981×10^5	1.0683×10^3	3.9266×10^5	1.1022×10^3
520–1260 (run 6)	0.8	7.1217×10^5	7.9738×10^2	4.7145×10^5	9.8217×10^2
	0.6	5.4088×10^5	1.0466×10^3	3.1280×10^5	1.2183×10^3
	0.4	4.7646×10^5	9.9457×10^2	2.8453×10^5	1.1067×10^3
520–1460 (run 7)	0.8	6.0127×10^5	9.5310×10^2	2.4086×10^5	1.1257×10^3
	0.6	4.8852×10^5	9.4961×10^2	1.9817×10^5	1.0915×10^3
	0.4	4.1156×10^5	8.3044×10^2	2.2610×10^5	9.2656×10^2

diffusivity was observed after each annealing cycle. The results obtained at the three radial positions show that the thermal diffusivity increases from the pellet periphery to the centre (Fig. 4). The thermal diffusivity at about 520 K before annealing is lowest close to the pellet rim ($\alpha \approx 6.2 \times 10^{-7}\ m^2 \times s^{-1}$ at $r/r_0 = 0.8$) and the value increases as the centre of the pellet is approached ($\alpha \approx 6.7 \times 10^{-7}\ m^2 \times s^{-1}$ at $r/r_0 = 0.6$ and $\approx 8.0 \times 10^{-7}\ m^2 \times s^{-1}$ at $r/r_0 = 0.4$). The same radial dependence is also found after annealing at 1460 K: the thermal diffusivity at about 520 K is lowest close to the pellet rim: $\alpha \approx 1.18 \times 10^{-6}\ m^2 \times s^{-1}$ at $r/r_0 = 0.8$, it is $\approx 1.28 \times 10^{-6}\ m^2 \times s^{-1}$ at $r/r_0 = 0.6$ and $1.40 \times 10^{-6}\ m^2 \times s^{-1}$ at $r/r_0 = 0.4$. The thermal diffusivity values were fitted to the function $1/(A + BT)$. The values of the coefficients A and B are given in Table 1.

4.2. Thermal conductivity

The local thermal conductivity $\lambda(T) = \rho(T)\, C_p(T)\, \alpha(T)$ was calculated from the local thermal diffusivity, $\alpha(T)$, the heat capacity, $C_p(T)$, and the local density, $\rho(T)$. The pellet average porosity fraction is 0.05 and the local values are estimated to be 0.05, 0.04 and 0.04 at the relative radial positions $r/r_0 = 0.8$, 0.6 and 0.4, respectively. Taking into account the measurement uncertainties, the local porosity fractions can be considered as equal to 0.05 for the three positions. The irradiation temperatures were calculated to be 880, 1000 and 1080 K, respectively. The specific heat, C_p, was assumed to be equal to the value for fresh MOX fuel as given by Duriez et al. [1]. The density at 300 K at the measurement radial positions was taken to be 10.31 $g \times cm^{-3}$, which is the pellet average. The relation recommended by Martin for the thermal expansion [10] was used to calculate the density as a function of temperature. Considering the uncertainties on the thermal diffusivity (5%), specific heat (2%) and density (3%), the uncertainty on the thermal conductivity over the whole temperature range is of 10%.

The thermal conductivity curves obtained at $r/r_0 = 0.6$ (i) up to the irradiation temperature, (ii) after annealing at the irradiation temperature and (iii) after annealing at 1460 K, are shown in Fig. 5. The behaviour of the thermal conductivity follows that of the thermal diffusivity.

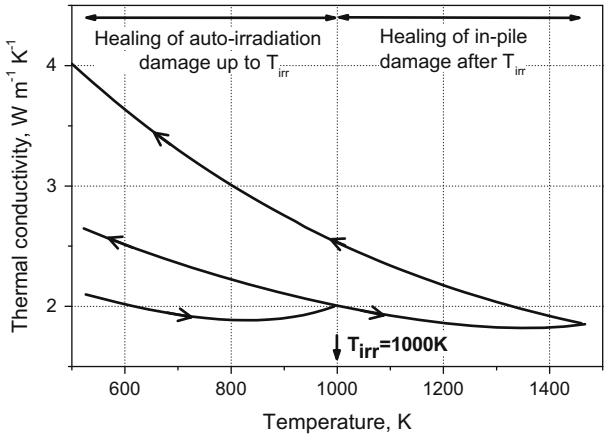

Fig. 5. Thermal conductivity below and above the irradiation temperature, at the radial position $r/r_0 = 0.6$.

Thermal conductivity values obtained by laboratory measurements, a considerable time after the end of the irradiation, are not the same as the end-of-life values since they include the effect of supplementary damage produced by auto-irradiation during storage. The first curve represents the conductivity measured on increasing the temperature up to the irradiation temperature. During this phase, only damage produced by the out-of-pile auto-irradiation is progressively annealed. The recovered conductivity is given by the curve obtained during the descending temperature measurement made immediately after this annealing. This corresponds to the first part of the second curve, when the measurement begins at low temperature and continues up to 1460 K. During this phase, the radiation damage produced in-pile is progressively annealed above the irradiation temperature. The third curve represents the conductivity of the sample after annealing at 1460 K. Thermal conductivity values at the radial position $r/r_0 = 0.8$ (close to pellet rim) are given in Table 2.

Only the measurements at the irradiation temperature truly represent the state of the fuel in-pile, because different irradiation

Table 2
Experimental thermal conductivity at the radial position $r/r_0 = 0.8$ (close to pellet rim).

T (K)	Thermal conductivity ascending up to irradiation temp. ($W\,m^{-1}\,K^{-1}$)	T (K)	Thermal conductivity ascending after annealing at irradiation temp. ($W\,m^{-1}\,K^{-1}$)	T (K)	Thermal conductivity descending after annealing at 1460 K ($W\,m^{-1}\,K^{-1}$)
539	1.90	531	2.35	1460	1.73
633	1.92	756	2.14	1346	1.90
755	1.90	936	1.95	1106	2.24
829	1.89	1030	2.07	758	2.96
936	1.95	1020	2.01	522	3.58
		1110	1.93		
		1190	1.82		
		1350	1.76		
		1460	1.73		

temperatures lead to differences in microstructure and damage state [11]. The dynamical damage produced in-pile during the fissions spikes is also absent. Furthermore, this interpretation supposes that the damage produced by auto-irradiation can clearly be distinguished and separated from that produced in-pile. In fact both are of the same nature (point defects like interstitials and vacancies and extended defects like voids and dislocations) but are produced at different temperatures. In-pile, the radiation damage that can be removed at temperatures lower than the irradiation temperature is immediately healed, and the damage not annealed out at this temperature survives with saturation concentrations at the irradiation temperature. Therefore, auto-irradiation should not produce supplementary damage annealable at temperatures higher than the irradiation temperature, because of the in-pile saturation of such damage. However, as auto-irradiation takes place at lower temperature, the saturation threshold for the different point and extended defects is higher than at the irradiation temperature and auto-irradiation might produce damage annealable at temperatures higher than the irradiation temperature. This contribution requires supplementary modelling work and is neglected here. The defects restoration is not the only phenomena taking place during thermal annealing: the fission gas distribution within the fuel evolves starting at about 1150 K. The fission gas atoms diffuse from the fuel matrix and precipitate into bubbles or are released. While the gas diffusion from the fuel matrix is expected to have a positive effect on the thermal conductivity, degradation results from the swelling. The thermal diffusivity measurements alone are not sufficient in order to make a distinction between these effects.

5. Comparison with literature data for UO_2 and MOX

The thermophysical properties and in-pile performance of MOX and UO_2 fuels are usually compared in order to assess the effect of the addition of Pu. In the normal operating temperature range of the fuel (600–1500 K), the thermal conductivity of uranium and plutonium dioxide is dominated by a phonon heat transport mechanism that is described by the simple relationship $1/(A + BT)$. Both A and B are modified by irradiation. The temperature dependent term, B, represents the phonon–phonon interaction and is referred as the *Umklapp* process, resulting in a linear relationship between the thermal resistivity and T. The A coefficient is linked to the concentration of phonon scattering centres; particularly lattice point defects (vacancies and interstitials resulting from irradiation damage). The substitutional and accommodated atoms produced by fission that replace U, Pu or O atoms in the lattice or are hosted at interstitial positions constitute additional scattering centres for phonons. Linear defects (such as dislocations) are less effective scattering centres because they impose much weaker local strain on the lattice. Larger discontinuities such as porosity, bubbles, and solid precipitates have the least phonon scattering efficiency.

The thermal conductivity of un-irradiated MOX was found to be significantly lower than that of UO_2. This decrease is usually attributed to the differences in atomic mass and ionic radius between the U^{4+} and Pu^{4+} cations [1]. Duriez et al. [1] and Gibby [2] made systematic measurements of the thermal conductivity of fresh MOX fuel and have found that the effect of the Pu concentration is negligible in the range 3–15 wt.%. This observation is hardly compatible with a pure Pu concentration effect and an alternative interpretation including the stoichiometry fluctuations was proposed [3]. In the heterogeneous MOX and for a given oxygen potential corresponding for instance to a O/M value of 2.00, non stoichiometric regions coexist with levels depending on the local Pu concentration. The degree of homogeneity of the Pu distribution was found to have no significant effect [1]. Similar comparisons for irradiated fuels are not available in the open literature.

Before considering the measurement results of the irradiated fuel, the effect of damage caused by auto-irradiation in fresh fuels during storage needs to be considered. Self-irradiation produces point or extended defects during storage, even before the fuel is irradiated. The amount of damage generated depends on the irradiation dose accumulated. Self-irradiation damage lowers the thermal conductivity of fresh fuels [12]. Starting from a damaged fuel, the thermal conductivity measurements performed after different annealing cycles (increase of the maximum temperature in each cycle) reveal a progressive recovery as a function of the temperature. The different annealing stages and the nature of the related defects were shown to be identical in auto-irradiated and reactor-irradiated fuels [12].

1. Oxygen vacancy/interstitial recombination (oxygen Frenkel pairs) at 600–800 K.
2. Recombination of uranium vacancy/interstitial clusters at 800–1000 K.
3. Dislocation loop formation near 1100 K.
4. Precipitation of voids near 1150 K followed by fission gas redistribution (bubble formation with partial gas sweeping from the matrix).

The evolution of the stoichiometry during irradiation is another parameter affecting the thermal conductivity. Oxygen potential measurements have shown that for irradiated MOX fuel the value is in the range $-400\,kJ\,mol^{-1}$ at 500 K and $-300\,kJ\,mol^{-1}$ at 1300 K, these values being dominated by fission products like Mo/MoO_2. According to the estimations of Ball [13] for fresh MOX fuel, this range corresponds to O/M between 2.001 and 2.01. The relative decrease in thermal conductivity due to non stoichiometry can be expected to be reduced in irradiated fuel as compared to fresh fuel because of the large number of defects produced by irradiation, including oxygen defects; however this statement requires further investigations.

The literature values of the thermal conductivity of irradiated UO_2 and MOX correspond to 95% of the theoretical density, which also corresponds to the experimental values obtained in this work (no porosity correction was necessary). The correction for porosity used by the different authors, as well as the porosity levels and pores shape may have an impact on the comparison, however these parameters were not re-assessed here and the final recommended values were used. The thermal conductivity of irradiated UO_2 has been deduced by Wiesenack [14] from on-line temperature measurements using thermocouples placed in the centre of fuel pellets during irradiation. The thermal conductivity of irradiated UO_2 was measured out-of-pile by Ronchi et al. [15] and Amaya et al. [16] using the laser flash technique. Differences may

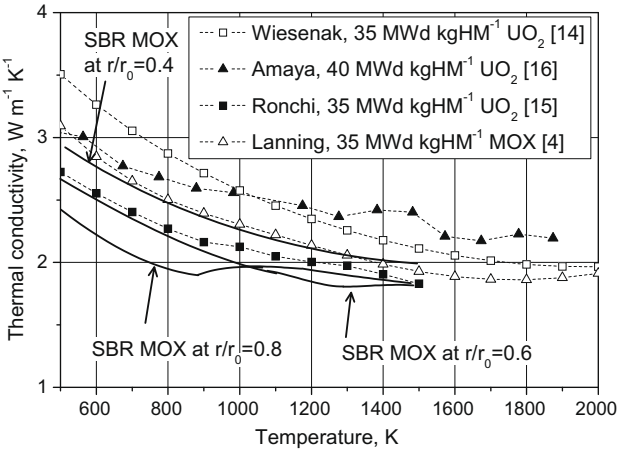

Fig. 6. Thermal conductivity of homogeneous SBR MOX fuel compared with literature data for irradiated UO_2 and homogeneous MOX fuel. Local burn-up 30 MWd/kgHM at $r/r_0 = 0.4$, 32 MWd/kgHM at $r/r_0 = 0.6$ and 35 MWd/kgHM at $r/r_0 = 0.8$.

exist in the oxygen potential control during the experiments, but the influence of this parameter is usually not quantified. For a burn-up of 35 MWd/kgHM, the values obtained with the correlation of Ronchi et al. [15] are the lowest, the values obtained with the correlation of Wiesenack [14] are higher below 1000 K (see Fig. 6). The experimental results of Amaya et al. [16] for UO_2 with 40 MWd/kgHM burn-up show a higher thermal conductivity than the values obtained with the correlation of Ronchi, especially at high temperatures (Fig. 6).

There are few publications on the thermal conductivity of irradiated MOX fuels. For the irradiated low Pu content MOX (3–15 wt.%), Lanning [4] proposed a formula based on the results obtained for fresh MOX by Duriez et al. [1] adding the degradation of the thermal conductivity as a function of burn-up, assuming that this is similar to that for UO_2 fuel obtained by Ohira and Itagaki [17]. This correlation predicts that at a burn-up of 35 MWd/kgHM, the thermal conductivity of irradiated MOX is in the same range as that of irradiated UO_2 predicted by the correlation of Ronchi (see Fig. 6).

The experimental results obtained for SBR MOX fuel after annealing at the irradiation temperature and reported in this paper are compared with the literature data in Fig. 6. Below 1000 K, the UO_2 thermal conductivity from in-pile measurements [14] is noticeably higher than those measured out-of-pile. The values of Lanning for homogeneous MOX lie between the two UO_2 curves. The deviation between the data from different sources decreases with increase in temperature, and above 1500 K the thermal conductivity curves converge. The best agreement with the new measurements is obtained with the correlation of Ronchi determined from results for UO_2 obtained with the same equipment. It is seen from Fig. 6 that the conductivity obtained in the outer region of the fuel is slightly lower than that of UO_2, while the conductivity in the central region of the fuel is slightly higher. The conductivity obtained at mid-radius is almost equal to that of UO_2. Taking into account the experimental uncertainties, it is recommended that the Ronchi UO_2 correlation should be used to predict the thermal conductivity of irradiated MOX with burn-ups around 35 MWd/kgHM. The predictions obtained with the formula of Lanning are slightly higher but remain acceptable.

6. Summary

Experimental results for the thermal conductivity of irradiated nuclear fuels are scarce and the correlations for UO_2 and MOX in the literature give significantly different predictions. In this paper, thermal diffusivity measurements performed on irradiated SBR MOX with a burn-up of 35 MWd/kgHM have been presented. The microstructure of the SBR MOX fuel is characterised by a homogeneous Pu distribution with less than 2 vol.% of Pu rich spots. The thermal diffusivity and its variation during laboratory annealing have been interpreted in terms of the local burn-up, local irradiation temperature and local porosity. The supplementary effect of the damage produced by auto-irradiation in the time interval between the end of irradiation and the measurement was assessed. This aspect is particularly important for the irradiated MOX fuel because its alpha activity is higher than for UO_2. The thermal diffusivity dependence on the radial position was quantified by making measurements at three radial positions: close to the pellet rim, approximately at mid-radius, and closer to the pellet centre. The deduced thermal conductivity at 520 K was found to decrease from 2.9 $Wm^{-1}K^{-1}$ close to the pellet centre to 2.4 $Wm^{-1}K^{-1}$ close to the pellet rim. This decrease is due to the increase of the burn-up and to the decrease of irradiation temperature.

These results were compared with those of previously published measurements or correlation functions for the irradiated UO_2 and MOX fuels. Comparison with recent measurements on UO_2 [15] shows that the thermal conductivity of homogeneous SBR MOX fuel at a burn-up of 35 MWd/kgHM is not significantly different from that of the UO_2 with the same burn-up. The addition of a few percent of Pu in UO_2 lowers the thermal conductivity of the fresh fuel but does not significantly alter the thermal conductivity in the irradiated state. The influence of the Pu is progressively reduced by the irradiation effects and by the convergence of the compositions of the fuels due to the consumption of Pu in the MOX and to the formation of Pu in the UO_2 fuel. Supplementary measurements are planned in order to check this statement for heterogeneous MOX fuels, in which the burn-up is less homogeneous because of the larger fraction of Pu-rich areas.

Acknowledgements

The authors would like to thank Sellafield Ltd. (formerly part of the BNFL group) for providing the fuel used in this study.

References

[1] C. Duriez, J.P. Alessandri, T. Gervais, Y. Philipponneau, J. Nucl. Mater. 277 (2000) 143.
[2] R.L. Gibby, J. Nucl. Mater. 38 (1971) 163–177.
[3] D. Baron, in: Proc. OECD/NEA Seminar on Thermal Performance of High Burn-up LWR Fuel, Cadarache, France, March 1998, p. 99.
[4] D.D. Lanning, C.E. Beyer, K.J. Greelhood, in: Proc. ANS Int. Mtg. on LWR Fuel Performance, Orlando, 2004.
[5] H. Fujii, H. Teshima, K. Kanasugi, T. Sendo, J. Nucl. Sci. Technol. 43 (9) (2006) 998.
[6] R.J. White, S.B. Fisher, P.M.A. Cook, R. Stratton, C.T. Walker, I.D. Palmer, J. Nucl. Mater. 288 (2001) 43.
[7] S.B. Fisher, R.J. White, P.M.A. Cook, S. Bremier, R.C. Corcoran, R. Stratton, C.T. Walker, P.K. Ivison, I.D. Palmer, J. Nucl. Mater. 306 (2002) 153.
[8] P.A. Jackson, J.A. Turnbull, R.J. White, Nucl. Energy 29 (1990) 107.
[9] M. Sheindlin, D. Halton, M. Musella, C. Ronchi, Rev. Scient. Instr. 69 (3) (1998) 1426.
[10] D.G. Martin, J. Nucl. Mater. 94 (1988) 152.
[11] C.E. Beyer, D.D. Lanning, in: Proc. OECD/NEA Seminar on Thermal Performance of High Burn-up LWR Fuel, Cadarache, France, March 1998.
[12] D. Staicu, T. Wiss, V.V. Rondinella, J.P. Hiernaut, R.J.M. Konings, C. Ronchi, J. Nucl. Mater. 397 (2010) 8.
[13] R.G.J. Ball, Report AERE R, 1989, p. 13395.
[14] W. Wiesenack, in: Proc. ANS Int. Mtg. on LWR Fuel Performance, Portland, Oregon, USA, 1997, p. 507.
[15] C. Ronchi, M. Sheindlin, D. Staicu, M. Kinoshita, J. Nucl. Mater. 327 (2004) 58.
[16] M. Amaya, M. Hirai, H. Sakurai, M.S.K. Ito, T. Nomata, K. Kamimura, R. Iwasaki, J.N. Mater, J. Nucl. Mater. 300 (2002) 57.
[17] K. Ohira and N. Itagaki. in: Proc. ANS Int. Mtg. on LWR Fuel Performance, Portland, Oregon, 1997.